2010 IEEE International Conference on Robotics and Automation
Anchorage Convention District
May 3-8, 2010, Anchorage, Alaska, USA

Flexible Space Robotic Manipulator with Passively Switching Free Joint to Drive Joint

Masatsugu Otsuki

Abstract— **This paper presents the manipulator with the new joint which can passively switch free state to drive state and vice versa. The manipulator with the free-state joint is categorized as a system subjected to a nonholonomic constraint; hence, its smooth feedback control cannot be implemented. In this paper, the issues on its control are clarified through the test with the experimental setup of the manipulator with a free joint. The manipulator with the switching joint is also developed and its effectiveness is verified through the experiment. Consequently, the trivial actuation using the proposed joint accomplishes more precise positioning in the experiment.**

I. Introduction

In lunar or planetary exploration, a longer, more lightweight, quicker and more forceful manipulator with low power consumption is always demanded for sampling materials around a lander and a rover, and laying scientific instruments on planetary surface. For the design of the manipulator like that, some requirements often introduce the trade-off such as flexibility of a link and reached distance, and torque and quickness. Thus, the nonconventional approach is required to solve these conflicts in the space robotic manipulator. Meanwhile, a control problem of a manipulator with a non-drive joint such as Under-Actuated Manipulator (UAM), which has acceleration nonholonomic constraint, attracts attention by many researchers. There are some advantages in UAM, such as lightweight of link, lower energy for driving it, small reactive torque to a attached base, as compared to the manipulator with actuated joints; in particular, UAM is suitable for use in space. Oriolo shows that a manipulator with the free joint is a type of the system with the second order nonholonomic constraint [1]. A control theory for a linear approximation system such as an inverted pendulum system cannot be applied to this system because it is a type of system which cannot accept a smooth feedback control [2]. For this system, there have been many studies such as the control of the robot arm with the free joint using periodic input by Nakamura [3], the control using impulsive force by Arai [4], and the stability analysis for the Chained System by Kobayashi[5]. However, it is practically difficult for UAM to perform precise positioning for the manipulator at the end of its motion.

Therefore, we propose the space robotic manipulator with the new joint, which can passively switch drive and free states, for implementing the precise positioning. In addition of the precise positioning, fault tolerance in the switch joint can be expected because the joint can be driven in both free and drive states. However, since the new mechanism is involved in the joint, the weight is slightly increased. Hence, this disadvantage in the passively switching joint is also verified on the basis of the experimental results in this paper. Firstly, the issues on the control of UAM are clarified through the test with the experimental setup of the manipulator with a free joint. Secondly, the manipulator with the switching joint is also developed and its effectiveness is examined through the experiment.

Masatsugu Otsuki is with Institute of Space and Astronautical Science, Japan Aerospace Exploration Agency, 3-1-1, Yoshinodai, Sagamihara-shi, Kanagawa, Japan otsuki.masatsugu@jaxa.jp

II. Awareness of the problem on control of UAM

It is shown in this section that the optimal trajectory planning method for UAM with lightweight links and we will be aware of the issues on its control.

A. The controlled object

The two link manipulator with a free, a driving and a payload, as shown in Fig.1 is considered as the examined controlled object. The first joint is actuated by the DC brushed motor and the second joint moves freely; in addition, the second and payload joints equip with levitation devices. The DC motor, which is controlled by using the digital signal processor, and an encoder are included in the actuated joint. In the free joint, the encoder and absolute position sensor, which is based on a positioning sensitive device (PSD), are located; and PSD is also attached to the top of the payload. The encoder measures the rotation angle of all the joints and the bending angles at both ends of the link are then calculated on the basis of the measurement by PSD. Furthermore, in order to let the first and second links be flexible, the drive and free joints are connected by using a thin aluminum plate, and the free and payload joints are connected by using the super-light flexible link, which made of piano wire. The first link is made by the aluminum flat plate and its weight is 5.0×10^{-2} kg. The second one is made of the piano wire whose weight is 4.0×10^{-3} kg.

B. Introduction for the equation of motion and state equation

In this section, the manipulator is formulated on the basis of the schematic in Fig.2. First, the bending due to flexibility of the link is approximated on the basis of the static bending curve by Shimoyama [6]. This model can express the behavior with low order vibration mode and the forced deflection by the actuator. The link of the controlled object in this study is very light as compared to the weight of joint, and the vibration modes till the second order are appeared; thus, the static bending curve is adequate for the

Fig. 1. Experimental setup of manipulator with two lightweight links and a free joint

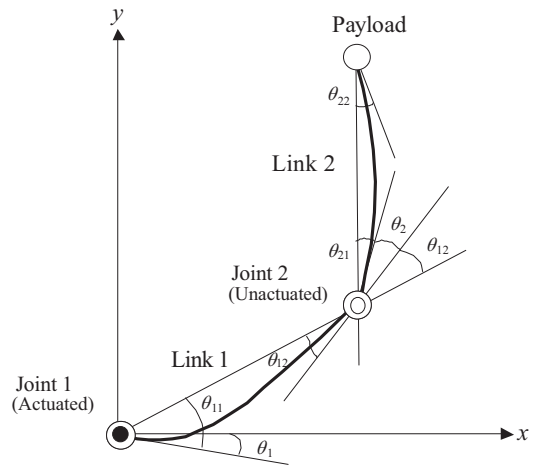

Fig. 2. Schematic representation of 2-link flexible manipulator

model which expresses the deflection in the flexible link. The bending angle of each joint, which receives the momentum at both ends, is derived from the following equation based on the beam formula.

$$\theta_{i1} = \frac{Mo_{i1}}{3E_iI_i}l_i + \frac{Mo_{i2}}{6E_iI_i}l_i,\ \ \theta_{i2} = \frac{Mo_{i1}}{6E_iI_i}l_i + \frac{Mo_{i2}}{3E_iI_i}l_i \quad (1)$$

where $i = 1, 2$ and Mo_{ij} are the rotational momentum at the place where the bending angle θ_{ij} occurs. The first joint is actuated and the second one is free; thus, the value of the momentum for θ_{11} is adequately larger than that for θ_{12}. And the second joint and payload are then connected to the free joint; namely, the momentum for θ_{21} and θ_{22} is almost identical. Hence, the momentum against both ends of the flexible link can be described by the following equation.

$$Mo_{11} >> Mo_{12},\ \ Mo_{12} = Mo_{22} \quad (2)$$

Further, Eq.(2) introduces the equation for the bending angle at both ends of each link as follows.

$$\theta_{11} = \frac{Mo_{11}}{3E_1I_1}l_1,\ \theta_{12} = \frac{Mo_{11}}{6E_1I_1}l_1,$$
$$\theta_{21} = \frac{Mo_{21}}{2E_2I_2}l_2,\ \theta_{22} = \frac{Mo_{21}}{2E_2I_2}l_2 \quad (3)$$

From the aforementioned equations, the bending angles have the following relation.

$$\theta_{11} = 2\theta_{12},\ \ \theta_{21} = \theta_{22} \quad (4)$$

It is defined that the position at the second joint is (x_1, y_1) and the position at the payload is (x_2, y_2) as shown in Fig.2.

The kinetic energy for the controlled object is calculated by

$$T = \frac{1}{2}m_1\left(\dot{x}_1^2 + \dot{y}_1^2\right) + \frac{1}{2}m_2\left(\dot{x}_2^2 + \dot{y}_2^2\right) + \frac{1}{2}J_{11}\left(\dot{\varphi}_1 + \dot{\theta}_{12}\right)^2 + \frac{1}{2}J_{21}\left(\dot{\varphi}_2 + \dot{\theta}_{22}\right)^2 + \frac{1}{2}J_1\dot{\theta}_1^2 + \frac{1}{2}J_2\left(\dot{\theta}_1 + \dot{\theta}_2\right)^2, \quad (5)$$

the potential energy is

$$U = \frac{3E_1I_1}{2l_1}\theta_{11}^2 + \frac{2E_2I_2}{l_2}\theta_{21}^2, \quad (6)$$

and the dissipative energy is given by the equation:

$$F = \frac{1}{2}c_{11}\dot{\theta}_{11}^2 + \frac{1}{2}c_{21}\dot{\theta}_{21}^2, \quad (7)$$

where $\varphi_1 = \theta_1 + \theta_{11}$ and $\varphi_2 = \varphi_1 + \theta_{12} + \theta_2 + \theta_{21}$. UAM is generally restricted by the non-holonimc constraint; thus, the equation of motion of the controlled object is introduced on the basis of the Lagrange equation with the constraint condition.

$$\frac{d}{dt}\left(\frac{\partial L}{\partial \dot{\theta}_k}\right) - \frac{\partial L}{\partial \theta_k} + \frac{\partial F}{\partial \dot{\theta}_k} = \tau_k\ \ (k = 1, \cdots, 4+m) \quad (8)$$
$$L = T - U + \sum_{j=1}^{m}\lambda_j C_j$$

In addition, m-equations for the nonholonomic constraint are described by the following:

$$\frac{\partial L}{\partial \lambda_j} = C_j = \sum_{k=1}^{4} A_{jk}\frac{d\theta_k}{dt} + A_j = 0\ \ (j = 1, \cdots, m), \quad (9)$$

where $\theta_3 = \theta_{11}$,$\theta_4 = \theta_{21}$; $\theta_{4+i} = \lambda_i\ \ (i = 1, \cdots, m)$; τ_k is the general force; m the number of the nonholonomic constraint; λ_j the Lagrange undetermined coefficient; and A_{jk} and A_j are the function of the time and general coordination θ_k. For the equations of motion at $(k = 2, 3, 4)$, namely for free joint, the general force τ_k equals zero. Further, it is formed that $\sum_{j=1}^{m}\lambda_j A_{jk} = 0$; which is the mechanical constraint for the object. Consequently, on the basis of he energy functions above and the Lagrange equations $(k = 1, \cdots, 4)$ the equations of motion in drive and free joints are derived from

$$M_{11}(\theta)\ddot{\theta}_a + \boldsymbol{M}_{12}(\theta)\ddot{\theta}_p + h_a(\theta, \dot{\theta}) + c_a(\theta) = \tau \quad (10)$$
$$\boldsymbol{M}_{21}(\theta)\ddot{\theta}_a + \boldsymbol{M}_{22}(\theta)\ddot{\theta}_p + \boldsymbol{h}_p(\theta, \dot{\theta}) + \boldsymbol{c}_p(\theta) = \boldsymbol{0} \quad (11)$$

where $\theta_a = \theta_1$, $\theta_p = [\theta_2\ \theta_3\ \theta_4]^T$, $\theta = [\theta_a\ \theta_p]^T$, $\boldsymbol{M}_{ij}$ $(i, j = 1, 2)$, and h_a, $\boldsymbol{h}_p$, c_a, $\boldsymbol{c}_p$ are the matrices which express inertia, Coriolis and centrifugal force, gravity terms, respectively. Moreover, τ is the torque which the actuated joint generates. Here, it is assumed that τ can adequately generate torque and the angular acceleration at the drive joint is employed as an input to the system; that is $u = \ddot{\theta}_1$. Consequently, τ is removed from the equation and the controlled system is expressed in the affine form:

$$\dot{\boldsymbol{x}} = \boldsymbol{g}(\boldsymbol{x}) + \boldsymbol{h}(\boldsymbol{x})u \quad (12)$$
$$\boldsymbol{g}(\boldsymbol{x}) = \begin{bmatrix} \dot{\theta}_a \\ \dot{\theta}_p \\ 0 \\ -\boldsymbol{M}_{22}^{-1}\left(\boldsymbol{h}_p + \boldsymbol{c}_p\right) \end{bmatrix},\ \boldsymbol{h}(\boldsymbol{x}) = \begin{bmatrix} 0 \\ \boldsymbol{0} \\ 1 \\ -\boldsymbol{M}_{22}^{-1}\boldsymbol{M}_{21} \end{bmatrix}$$

where $\boldsymbol{x} = \begin{bmatrix}\theta & \dot{\theta}\end{bmatrix}^T$ and the torque τ^o to implements the required angular acceleration u^o is calculated by the equation:

$$\tau^o = h_a + c_a - \boldsymbol{M}_{22}^{-1}\left(\boldsymbol{h}_p + \boldsymbol{c}_p\right) + \left(M_{11} - \boldsymbol{M}_{12}\boldsymbol{M}_{22}^{-1}\boldsymbol{M}_{21}\right) u^o \tag{13}$$

C. Trajectory planning method

The extended Fourier basis algorithm [7] is employed for the trajectory planning method for UAM in this study. This method is obtained by extending the method by Fernandes [8] to the method which can apply to an affine system. The optimal trajectory for the actuated joint up to the target consists of the Fourier series, and the Newton method then directly introduces the coefficients of the Fourier series. The trajectory planning for the manipulator with the free joint is accomplished by following the calculated optimal trajectory with a casual control theory.

1) Conversion to parameter optimization problem: First, we consider the problem to calculate the input on the Hilbert space, which minimizes the following criterion function for $[t_0, t_f]$.

$$J(u) = \boldsymbol{e}_f^T \boldsymbol{M}_w \boldsymbol{e}_f + \int_{t_0}^{t_f} u(t)^T u(t) dt \tag{14}$$

$$\boldsymbol{e}_f = [\boldsymbol{x}(t_f) - \boldsymbol{x}_d] \tag{15}$$

where $\boldsymbol{M}_w$ is the nonnegative diagonal matrix and $\boldsymbol{x}_d$ is the target of the system state at the end of control. Since the controlled object is a type of nonlinear system, the optimization problem for the criterion function above is converted into the two-point boundary value problem. Consequently, it is complicated to analytically solve the problem above. Hence, using the n-order Fourier basis with the orthogonality of the Fourier basis e_i as

$$\int_{t_f}^{t_0} \boldsymbol{e}_i^T(t)\boldsymbol{e}_j(t) = \begin{cases} 0 & \text{if } i \neq j \\ 1 & \text{if } i = j, \end{cases} \tag{16}$$

the input $u(t)$ is given by the following equation:

$$\begin{aligned} u(t) &= \sum_{i=1}^{N} \alpha_i e_i(t) = \boldsymbol{E}(t)\alpha \\ &= \frac{1}{2}\alpha_1 + \sum_{j=1}^{n}\left[\alpha_{_{j+1}} cos\left(\frac{2\pi j t}{t_f}\right) + \alpha_{_{j+n+1}} sin\left(\frac{2\pi j t}{t_f}\right)\right] \end{aligned} \tag{17}$$

$$\alpha = [\alpha_1, \alpha_2, \cdots, \alpha_N] \tag{18}$$

$$\boldsymbol{E}(t) = [e_1(t), e_2(t), \cdots, e_N(t)] \tag{19}$$

where $N = 2n + 1$. Thus, the criterion function in Eq.(14) is rewritten as follows.

$$J(\alpha) = \boldsymbol{e}_f^T \boldsymbol{M}_w \boldsymbol{e}_f + < \alpha, \alpha > \tag{20}$$

Consequently, the subject to calculate the input on the infinite-order Hilbert space, which minimizes the criterion function in Eq.(14), results in the subject to calculate the parameters $\alpha_i\,(i = 1, 2, \cdots, N)$ on the N-order Euclid space, which minimize the criterion function in Eq.(20).

2) Optimizing algorithm: Second, in this section, using the algorithm based on the Newton method, the parameters $\alpha_i\,(i = 1, 2, \cdots, N)$ are optimized. With the Tailor expansion around α_k, the criterion function in Eq.(20) is converted into the following equation:

$$\begin{aligned} J(\alpha_k + \delta) =& J(\alpha_k) + \left\langle \left.\frac{\partial J}{\partial \alpha}\right|_{\alpha_k}, \delta \right\rangle \\ &+ \frac{1}{2}\left\langle \left.\frac{\partial^2 J}{\partial \alpha^2}\right|_{\alpha_k} \delta, \delta \right\rangle + o\left(\|\delta\|^3\right), \end{aligned} \tag{21}$$

$$\left.\frac{\partial J}{\partial \alpha}\right|_{\alpha_k} = 2\left(\alpha_k + \boldsymbol{Y}_f^T \boldsymbol{M}_w \boldsymbol{e}_f\right), \tag{22}$$

$$\left.\frac{\partial^2 J}{\partial \alpha^2}\right|_{\alpha_n} = 2\left[\boldsymbol{I} + \boldsymbol{Y}_f^T \boldsymbol{M}_w \boldsymbol{Y}_f + \sum_{i=1}^{N} \boldsymbol{Z}_{if} \boldsymbol{M}_w \boldsymbol{e}_f\right]. \tag{23}$$

where the matrices $\boldsymbol{Y}_f$ and $\boldsymbol{Z}_{if}$ are the terminal values of Jacobian of $\boldsymbol{x}(t)$ and Hessian of $x_i(t)$, which is i-th element of $\boldsymbol{x}(t)$, respectively, as follows.

$$\boldsymbol{Y}(t) = \frac{\partial \boldsymbol{x}(t)}{\partial \alpha}, \;\; \boldsymbol{Z}_i(t) = \frac{\partial^2 \boldsymbol{x}_i(t)}{\partial \alpha^2} \tag{24}$$

Substituting Eq.(17) into Eq.(12), the following equation is obtained.

$$\dot{\boldsymbol{x}} = \boldsymbol{g}(\boldsymbol{x}) + \boldsymbol{h}(\boldsymbol{x})u = \boldsymbol{g}(\boldsymbol{x}) + \boldsymbol{h}(\boldsymbol{x})\boldsymbol{E}(t)\alpha \tag{25}$$

Thus, by integrating the the derivative of $\boldsymbol{Y}(t)$:

$$\dot{\boldsymbol{Y}}(t) = \left[\frac{\partial \boldsymbol{h}(\boldsymbol{x})}{\partial \boldsymbol{x}} u + \frac{\partial \boldsymbol{g}(\boldsymbol{x})}{\partial \boldsymbol{x}}\right] \boldsymbol{Y}(t) + \boldsymbol{h}(\boldsymbol{x})\boldsymbol{E}(t), \tag{26}$$

with the initial value of $\boldsymbol{Y}(t)$:

$$\boldsymbol{Y}(0) = \lim_{t \to 0} \boldsymbol{Y}(t) = \boldsymbol{0}, \tag{27}$$

the terminal Jacobian $\boldsymbol{Y}_f$ is derived.

At this step, the update law based on the Newton method for repeatedly improving the Fourier coefficients α is expressed by the following equation with Eqs.(22) and (23).

$$\begin{aligned} \alpha^{n+1} =& \alpha^n - \mu\left[\boldsymbol{I} + \boldsymbol{Y}_f^T \boldsymbol{M}_w \boldsymbol{Y}_f + \sum_{i=1}^{N} \boldsymbol{Z}_{if} \boldsymbol{M}_w \boldsymbol{e}_f\right]^{-1} \\ &\times \left[\alpha^n + \boldsymbol{Y}_f^T \boldsymbol{M}_w \boldsymbol{e}_f\right] \end{aligned} \tag{28}$$

However, the update law of $alpha$ in this method is based on the following equation that Hessian $\boldsymbol{Z}_i(t)$ is omitted because of high computation load to calculating the Hessian matrix.

$$\alpha^{n+1} = \alpha^n - \mu\left[\boldsymbol{I} + \boldsymbol{Y}_f^T \boldsymbol{M}_w \boldsymbol{Y}_f\right]^{-1}\left[\alpha^n + \boldsymbol{Y}_f^T \boldsymbol{M}_w \boldsymbol{e}_f\right] \tag{29}$$

where $0 < \mu < 1$. Finally, by repeating the update law above, the parameter α^o for the quasi optimal trajectory is obtained.

D. The verification of the trajectory planning through the experimental test

In this section, we recognize the issues in the control for UAM through the test using the experimental setup.

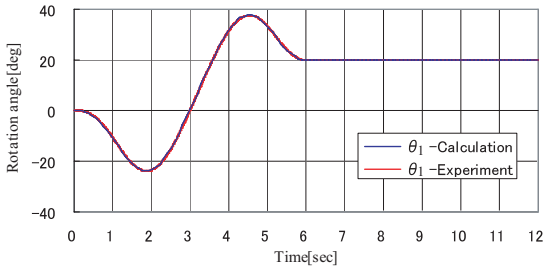

(a) Rotation angle of actuated joint

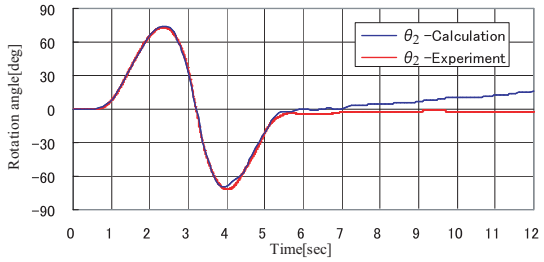

(b) Rotation angle of free joint

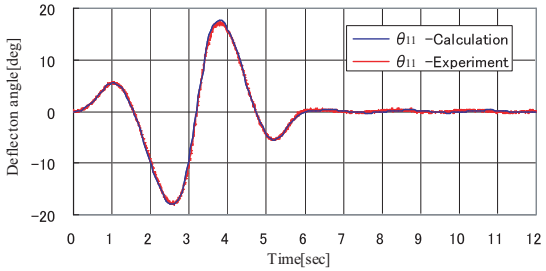

(c) Bending angle of flexible link attached to actuated joint

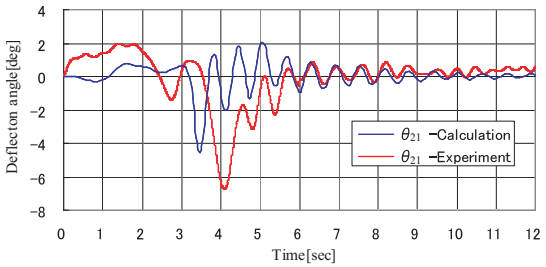

(d) Bending angle of flexible link attached to free joint

Fig. 3. Experimental results of positioning for the manipulator with two flexible links and a free joint

1) Conditions for experimental test: It is supposed that the initial angles of the drive and free joints are zero. The target angles of drive and free joints are 20 and 0 degrees, respectively. Further, the control is implemented until 6.0 second. The optimal trajectory up to the target is off-line calculated on the basis of the Fourier basis algorithm; additionally, the drive joint follows the calculated trajectory by using the PID control. The approximation order of the Fourier series is here assigned to be 3.

2) Consideration of the experimental results: Figures 3 (a), (b), (c) and (d) show the time histories of the angles in drive and free joints and bending angles of the first and second links, respectively. All figures consist of the results derived from the simulation and experimental test. Figures 3 (a), (b), (c) and (d) show that the behaviors of the drive joint and the first link in the experimental setup are equal to the behaviors obtained through the simulation. However, the rotation angle in the free joint through the experiment did not coincide with that of the simulation result; particularly, the error after stopping the motion is large. This means that the experimental setup has the actual problem such as friction in axis, approximation error of the Fourier basis and numerical error; as a result, they were not counted in the simulation. It is difficult to apply the complete solution to this problem. For example, if a clutch was equipped with the free joint, the rapid stop would cause the vibration of the second link. Therefore, the proposed passive switch joint can be expected to reduce the positioning error and vibration, simultaneously. Finally, in Fig.3(d), the results after large vibration occurs from the experimental test and simulation are largely different. This is due to the ignored high-order modes in the modeling of the simulation.

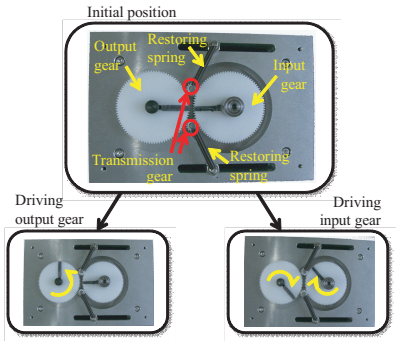

Fig. 4. The function of the passive switch joint

III. Experiment of Positioning of the Manipulator with the Switching Joint

This section shows the experiment using the setup with the new switchable joint, in which the precise positioning and suppression of the vibration by the proposed joint would be confirmed.

A. The function of the passive switch joint

The joint, which can switch the free state to drive state and vice versa, is key item for this study. Many switching mechanisms using an actuator and a ratchet exist; moreover, there are many mechanisms without an actuator to switch drive and lock states in one direction, such as a clutch. However, there are few mechanisms without an actuator to switch drive and lock/free states in both clockwise (CW) and counter-clockwise (CCW) directions. In this paper, we propose the simple mechanism to switch the drive state using a motor to the free state and vice versa, as shown in Fig.4. In this figure, the top view shows the initial position of

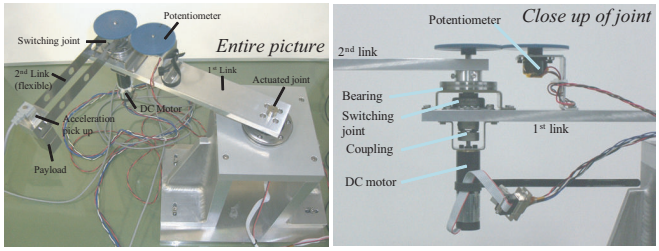

Fig. 5. Experimental setup of the manipulator with the switching joint

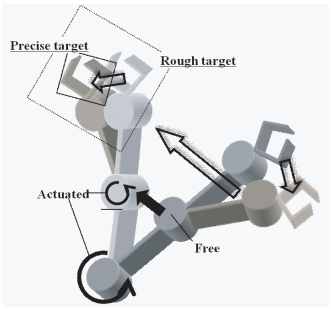

Fig. 6. The control schematic of the manipulator with passive switch joint

the proposed mechanism which consists of the four gears and two springs. Additionally, the bottom views show the state after actuating the gear at the output or input side. In the left figure at the bottom in Fig.4, the gear at the output side is actuated; however, the input side gear is not driven. Meanwhile, in the right figure, the gear at the input side is actuated; as the result, the output side gear is driven in the inverse direction with little phase delay. Naturally, the actuation for the input gear in the inverse direction can obtain the same result above. In this mechanism, the motion is governed by the transmission gears located between input and output side gears. Since the transmission gear is restored to the origin by the attached spring, the gear at the input side can actuate the transmission gear but the gear at the output cannot reach to the transmission gear. As the result, the proposed mechanism can accomplish to switch the drive and free modes without a switching actuator; thus, the manipulator with the characteristics of both UAM and manipulator with fully actuated joints can be developed. However, the following future studies are remained: 1) to reduce the phase delay due to backlash, and 2) to reduce size for actually implementing it to a joint. Therefore, the another switching device, which has the same function as the proposed mechanism above, is utilized in the experimental setup in this paper.

B. The experimental conditions

1) The experimental setup: The joint, which can passively select free and drive states, is involved in the experimental setup shown in Fig.5. The joint has some issues such as backlash in the future study. The actuated joint is moved by using the 20 Watt DC brushed motor and the switchable joint is driven with the 3.5 Watt one. The first link is extremely rigid and the second link is exchangeable; hence, it is changed into a rigid one or a flexible one. The payload is attached to the tip of the second link and its weight is approximately 0.19 kg.

2) The control scheme of the second joint: Positioning for this manipulator is composed by the two steps as shown in Fig.6. The first step is the rough position control of the manipulator based on the free state like UAM, and the second step is the precise position control based on the drive state. Thus, in this paper, the state of the second joint is simply switched at the time when the first joint is stopped. That is, the second joint and link start to move just after stopping the control of the first joint. Finally, the 2-DOF servo controller by Smith [9] is employed as the feedback controller.

3) The conditions: The test is performed in the two cases using rigid or flexible link for the second link. In each case: rigid '1' or flexible '2', the experiment with the three types of positioning, which are non-control in the second joint ('a' or 'Free'), to always control it ('b' or 'Full control') and to control it after the stop of the first joint ('c' or 'Control after stop'), is performed. And all the experiment is then started from 3 seconds.

C. The experimental results and consideration

For the case using the rigid link, the profile of the rotation angle in the second joint is appeared in Fig.7. In (1–a), the behavior of the second link is governed by the inertial force; that is, the behavior of the first link at the start and stop influences on the behavior of the second joint. Hence, in the duration just after start and stop of the first link, the second link is naturally moved in the inverse direction against the movement of the first link. Thus, in (1–c), the behavior of the second link is almost along (1–a) before the stop of the first joint; however, the second joint is driven after the stop and its angle can reach at the target. Meanwhile, in (1–b), the second link is always actuated by the motor; consequently, the second joint is moved so as to overcome the inertial force. However, there is overshoot due to the inertial force at the start and stop of the first link. Moreover, in Table. I which concludes the max current in the second motor, the max power consumption in the first motor in all the cases and the max acceleration at the tip of the second link, the max power consumption and current in (1–b) are larger than that in the other cases. Namely, the motor in the second joint always acts on the inertial force; thus, its reaction force influences on the first motor. For the case using the flexible link, the same results as the case using the rigid link are obtained as shown in Fig.8. Further, the vibration due to the flexibility of the second link increases the acceleration at the tip of the second link as shown in Fig.9. All the peak of the acceleration is appeared at the time when the second joint rebels against the inertial force on the second link due to the first link behavior. As the result, in (2–b), the acceleration has considerable peak but the vibration did not occur. The second link has extreme flexible; however, the amplitude of the vibration is small because of the nature of the free joint.

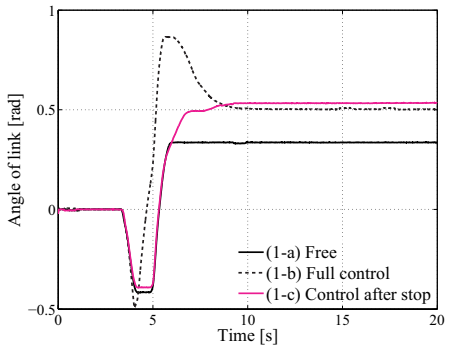

Fig. 7. Time history of the angle in the second joint of the manipulator with the rigid link

TABLE I

CONCLUSION OF THE EXPERIMENTAL RESULT

Case	Max current in the second motor [A]	Max power consumption in the first motor [W]	Max acceleration of tip in the second link $[m/s^2]$
1–a	0.00	1.42	–
1–b	0.239	2.99	–
1–c	0.105	1.13	–
2–a	0.00	2.74	2.18
2–b	0.270	5.66	6.76
2–c	0.161	2.29	2.22

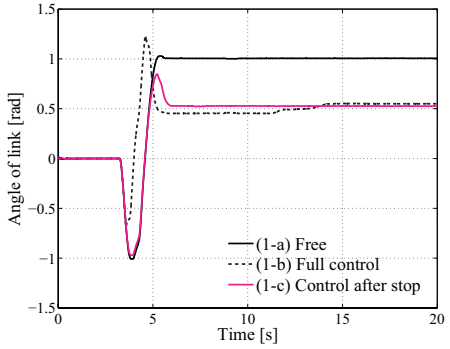

Fig. 8. Time history of the angle in the second joint of the manipulator with the flexible link

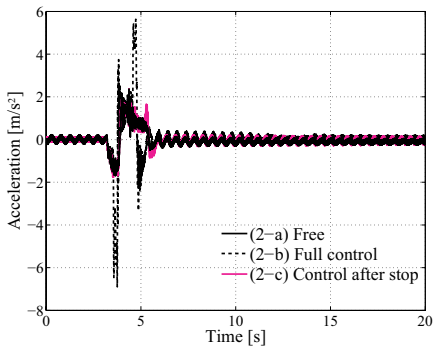

Fig. 9. Time history of acceleration at the tip of the second flexible link

D. Validation and future study

The weight of the switching joint is approximately 0.07 kg; thus, the weight of the manipulator is larger than that of the normal manipulator which has a motor by each joint. However, as shown in Table. I, the power consumption and max current are almost half of those in the full control case. As the result, the required performance, for the motor in joint, cables for the power line and a DC-DC converter, can descend and the weight of the whole system of the manipulator then extremely decreases. Meanwhile, the overshoot of the second link is appeared in (2–b). This is caused by the delay of the switching of the joint state. In this paper, the simple switching after the stop of the first joint is employed to change the state of joint. Therefore, in order to decrease the overshoot; that is, to more reduce the power consumption and current in the motor, the smooth switching method by the behavior of the free link is required as the future study.

IV. CONCLUSIONS

This paper presented the manipulator with the new joint which can passively switch free state to drive state and vice versa. The issues on its control were clarified through the test with the experimental setup of the manipulator with a free joint. The effectiveness of the manipulator with the switching joint was verified from the viewpoints of power consumption and vibration through the experiment. The trivial actuation using the proposed joint then accomplished precise positioning of the link subjected to the inertial force. In the future study, the performances to reduce the required power consumption and to suppress the vibration induced by inadequate switching will be enhanced by the smooth switching method.

ACKNOWLEDGMENT

This work was partially supported by MEXT, KAKENHI (20760153).

REFERENCES

[1] G. Oriolo, and Y. Nakamura, "Control of Mechanical Systems with Second-Order Nonholonomic Constraints:Underactuated Manipulators", *Proc.of the 1991 IEEE CDC*, pp.2398-2403, 1991

[2] H. Arai, "Nonholonomic control of underactuated manipulators", *J. Systems, control and information*, vol.43, no.10, pp.553-560, 1999

[3] Y. Nakamura, and R. Iwamoto, et al., "Control of nonholonomic mechanisms with drift", *J. the Robotics Society of Japan*, vol.13, no.6, pp.830-837, 1995

[4] H. Arai, and K. Tanie, et al., "Feedback control of a 3-axis planar manipulator with passive joint under a nonholonomic constraint", *J. the Robotics Society of Japan*, vol.15, no.6, pp.943-952, 1997

[5] K. Kobayashi, and J. Imura, et al., "Nonholonomic control of 3-D. O. F. manipulator with a free joint", *Trans. SICE*, vol.33, no.8, pp.799-804, 1997

[6] I. Shimoyama, and H. Miura, "A dynamic model for flexible manipulator control", *J. the Robotics Society of Japan*, vol.6, no.5, pp. 72-78, 1988

[7] M. Kamon, and K. Yoshida, "3D attitude control methods of free-flying dynamic system with initial angular momentum", *J. the Robotics Society of Japan*, vol.16, no.2, pp.223-231, 1998

[8] C. Fernandes, and L. Gurvits, et al., "Attitude Control of Space Platform/Manipulator System Using Internal Motion", *Proc. the 1992 IEEE International Conference on Robotics and Automation*, pp.893-898, 1992

[9] H. W. Smith and E. J. Davison, "Design of Industrial Regulators", *Proc. IEE*, vol. 119, pp.1210-1216, 1972.